REVERSIBLE ELECTRON BEAM HEATER FOR SUPPRESSION OF MICROBUNCHING INSTABILITIES BASED ON TRANSVERSE DEFLECTING CAVITIES*

Christopher Behrens (DESY, Hamburg, Germany),
Zhirong Huang, Dao Xiang (SLAC, Menlo Park, California)

Abstract

The presence of the microbunching instability due to the compression of high-brightness electron beams at existing and future X-ray free-electron lasers (FEL) results in restrictions on the attainable lasing performance and renders diagnostics like beam imaging with optical transition radiation impossible. The instability can be suppressed by introducing additional energy spread, i.e. heating the beam, as demonstrated by the successful operation of the laser heater system at the Linac Coherent Light Source. The increased energy spread is typically tolerable for self-amplified spontaneous emission FELs but limits the effectiveness of seeded FELs. In this paper, we present a reversible beam heating system based on two transverse deflecting cavities (TCAV) in front and behind a bunch compressor chicane. The additional energy spread will be introduced in the first TCAV, which suppresses the microbunching instability, and then will be eliminated in the second TCAV. We show the feasibility of the suppression of microbunching instabilities based on calculations and simulations, and set limits to the acceptable jitter tolerances.

INTRODUCTION

X-ray free-electron lasers (FELs) have become a reality with the successful operation of the Linac Coherent Light Source (LCLS) [1]. In order to suppress a microbunching instability associated with bunch compression that degrades the FEL performance, LCLS uses a laser heater to irreversibly increase the slice energy spread to a level tolerable for SASE operation [2]. For future X-ray FELs that plan to use external lasers to seed the FEL process in order to achieve better temporal coherence, a smaller slice energy spread is required to leave rooms for the additional energy modulation imprinted by the seed laser. Thus, the amount of tolerable heating is more restrictive and the longitudinal phase space control becomes more critical.

Transverse deflecting cavities (TCAVs) are routinely used for high-resolution temporal diagnostics in XFELs (e.g., Ref. [3]) and are proposed to use for novel beam manipulation methods (e.g., Ref. [4]). Recently, a transverse cavity was used to increase the slice energy spread (by off-axis longitudinal field) in an echo-enabled harmonic generation experiment at SLAC [5]. In this paper, we present a reversible beam heating system that uses two TCAVs located in front and behind a bunch compressor. The additional energy spread will be introduced in the first TCAV, which suppresses the microbunching instability, and then will be eliminated in the second TCAV. Simulations including coherent synchrotron radiation (CSR) and microbunching show the feasibility of this scheme to preserve both the transverse and longitudinal brightness of the electron beam.

* Work supported by DOE Contracts No. DE-AC02-76SF00515.

METHOD

In this and the following sections, we consider a linac employing a single bunch compressor for a soft x-ray FEL (such as the proposed linac configuration for the Next-Generation Light Source at LBL [6]). The choice of a single bunch compressor simplifies our consideration and analysis, although the concept may be applicable to a more typical double-compressor arrangement with some modifications. We note that a single bunch compressor arrangement has also been considered for the FERMI FEL in order to minimize the impact of microbunching instability [7].

Linear beam optics

In a transverse deflecting cavity, the transverse momentum gain is related to the transverse gradient of the longitudinal accelerating field through Panofsky-Wenzel theorem

$$\Delta p_y = -i\frac{e}{\omega}\int_0^L \nabla_y E_z dz\,, \tag{1}$$

where ω is the rf frequency, and L is the structure length.

Near the zero-crossing of the transverse deflecting cavity, we have

$$y' = \frac{e\omega V_y}{\gamma mc^3} z_0 \equiv \alpha z_0\,, \quad \delta = \alpha y_0\,, \tag{2}$$

where kick strength $\alpha = e\omega V_y/(\gamma mc^3)$, V_y is the peak deflecting voltage, and z_0 is the electron longitudinal position relative to TCAV zero crossing position, and y_0 is the electron vertical position relative to the TCAV axis. In the following we adopt the transport matrix notation of 6x6 matrix for $(x, x', y, y', z, \delta)$ but leaves (x, x') out for simplicity, i.e. (y, y', z, δ) will be used. The 4x4 transverse deflecting cavity matrix in the thin lens approximation is

$$\mathbf{R}_T^{thin} = \begin{pmatrix} 1 & 0 & 0 & 0 \\ 0 & 1 & \alpha & 0 \\ 0 & 0 & 1 & 0 \\ \alpha & 0 & 0 & 1 \end{pmatrix}. \tag{3}$$

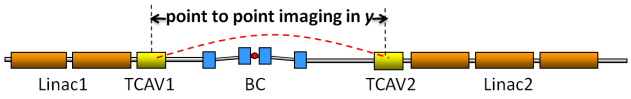

Figure 1: Schematic layout of a reversible heater system including two TCAV's, one in front and one behind a magnetic bunch compressor.

The reversible heater system shown in Fig. 1 consists of the following components: TCAV1 (with the kick strength α_1), a bunch compressor (with the momentum compaction factor R_{56}), TCAV2 (with the kick strength α_2). The vertical transport optics between TCAV1 and TCAV2 should be point to point imaging (i.e., satisfying $R_{34} = 0$ in 6x6 matrix notation). Including the momentum compaction from the bunch compressor, the 4x4 matrix between two transverse cavities is

$$\mathbf{R}_C = \begin{pmatrix} a & 0 & 0 & 0 \\ b & 1/a & 0 & 0 \\ 0 & 0 & 1 & R_{56} \\ 0 & 0 & 0 & 1 \end{pmatrix}, \tag{4}$$

where a is the magnification factor.

A linac section (Linac 1) before TCAV1 will introduce a linear chirp for compression (h), and the linac section after TCAV2 (Linac 2) will use an opposite chirp $-h/(1+hR_{56})$ to cancel the initial chirp. The entire matrix is

$$\begin{pmatrix} a & 0 & 0 & 0 \\ b+\alpha_1\alpha_2 R_{56} & \frac{1}{a} & \frac{\alpha_1}{a}+\alpha_2(1+hR_{56}) & \alpha_2 R_{56} \\ \alpha_1 R_{56} & 0 & 1+hR_{56} & R_{56} \\ \frac{\alpha_1}{1+hR_{56}}+a\alpha_2 & 0 & 0 & \frac{1}{1+hR_{56}} \end{pmatrix}. \tag{5}$$

We see that setting $\alpha_1/a + \alpha_2(1 + hR_{56}) = 0$ will cancel both the transverse kicks and induced energy spread.

Since TCAV1 kick strength is very weak and can be a short section, the thin lens approximation is valid. However, TCAV2 kick strength is usually stronger, and the effect of the finite cavity length should be taken into account. The symplectic matrix of a thick TCAV2 (with the length L_2) is [4]

$$\mathbf{R}_T^{thick} = \begin{pmatrix} 1 & L_2 & \alpha_2 L_2/2 & 0 \\ 0 & 1 & \alpha_2 & 0 \\ 0 & 0 & 1 & 0 \\ \alpha_2 & \alpha_2 L_2/2 & \alpha_2^2 L_2/6 & 1 \end{pmatrix}. \tag{6}$$

In this case, we should make sure the point to point imaging is from TCAV1 to the middle of TCAV2, and adjust the Linac 2 chirp to also cancel the TCAV2 induced energy chirp. After the straightforward matrix multiplication, the overall matrix after Linac 2 when $\alpha_1/a+\alpha_2(1+hR_{56}) = 0$ is

$$\begin{pmatrix} a+\frac{bL_2}{2}+\frac{\alpha_1\alpha_2 R_{56}L_2}{2} & \frac{L_2}{2a} & 0 & \frac{\alpha_2 L_2 R_{56}}{2} \\ b+\alpha_1\alpha_2 R_{56} & \frac{1}{a} & 0 & \alpha_2 R_{56} \\ \alpha_1 R_{56} & 0 & 1+hR_{56} & R_{56} \\ 0 & 0 & 0 & \frac{1}{1+hR_{56}} \end{pmatrix}. \tag{7}$$

Microbunching gain suppression

Although no additional energy spread is generated in the process, one can see that the density modulation can be suppressed by the $z-y$ coupling term in Eq. (7). Using the vector notation $(y_1, y_1', z_1, \delta_1)$ for particles in Linac 1, the longitudinal position in Linac 2 is

$$z_2 = \alpha_1 R_{56} y_1 + (1 + hR_{56}) z_1 + R_{56}\delta_1 \,. \tag{8}$$

Suppose that $\delta_1 = \delta_0 + \delta_m$, where δ_0 is the uncorrelated energy deviation, and $\delta_m(z_1)$ is the energy modulation accumulated before and in Linac 1. Following Ref. [8], the initial energy modulation at the wavelength k_1 is converted into additional density modulation at a compressed wavenumber k_2. For a 4-D distribution function $F(y_2, y_2', z_2, \delta_2)$, the bunching factor is given by

$$\begin{aligned} b_f(k_2) &= \int dy_2 dy_2' dz_2 d\delta_2 e^{-ik_2 z_2} F(y_2, y_2', z_2, \delta_2) \\ &= \int dy_1 dy_1' dz_1 d\delta_0 e^{-ik_2\alpha_1 R_{56} y_1 - ik_2(1+hR_{56})z_1} \\ &\quad e^{-ik_2 R_{56}(\delta_0+\delta_m(z_1))} F_0(y_1, y_1', z_1, \delta_0)\,, \end{aligned} \tag{9}$$

where $F_0(y_1, y_1', z_1, \delta_0)$ is the initial 4-D distribution. If the induced energy modulation is small such that $|k_2 R_{56}\delta_m| \ll 1$, we expand the exponent of Eq. (9) up to the first order in δ_m to obtain

$$\begin{aligned} b_f(k_2) \approx & b_0(k_1) - ik_2 R_{56} \int dz_1 \delta_m(z_1) e^{-ik_1 z_1} \\ & \times \int dy_1 d\delta_0 e^{-ik_2\alpha_1 R_{56} y_1 - ik_2 R_{56}\delta_0} U(y_1) V(\delta_0)\,, \end{aligned} \tag{10}$$

where $k_2 = Ck_1$, $C = 1/(1 + hR_{56})$, $U(y_1)$ describes the transverse profile, and $V(\delta_0)$ is the initial energy distribution. For both Gaussian profiles,we have

$$\begin{aligned} b_f(k_2) = b_0(k_1) - & ik_2 R_{56}\delta_m(k_1) \exp\left[-(k_2^2 R_{56}^2 \alpha_1^2 \sigma_{y1}^2/2)\right] \\ & \times \exp\left[-(k_2^2 R_{56}^2 \sigma_{\delta 0}^2/2)\right]\,. \end{aligned} \tag{11}$$

Here we denote the Fourier transform of $\delta_m(z_1)$ as $\delta_m(k_1)$, which is the accumulated energy modulation at the wavenumber k_1 in Linac-1 due to longitudinal space charge and other collective effects. $\sigma_{\delta 0} = \sigma_\gamma/\gamma$ is the initial slice energy spread, and σ_{y1} is the vertical beam size in TCAV1. We see that $\alpha_1\sigma_{y1}$ acts like effective energy spread for microbunching gain suppression.

NUMERICAL ILLUSTRATIONS

We demonstrate the feasibility of the reversible heater system using the following bunch compression example that is similar to the compressor configuration presented in Ref. [6]. Table 1 summarizes the main parameters used in the simulations. The adopted optics model, including the TCAV positions, is shown in Fig. 2.

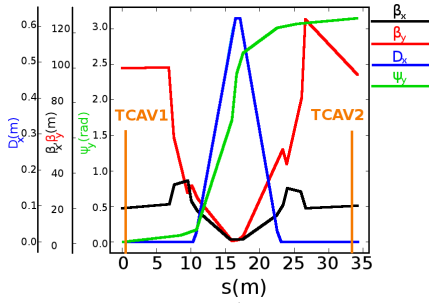

Figure 2: Accelerator optics (Twiss parameters) used to demonstrate the reversible heating system.

Table 1: Beam, bunch compressor, and TCAV parameters used to demonstrate the reversible heating system.

Parameter	Symbol	Value	Unit
Beam energy	γmc^2	350	MeV
Init. transv. emittance	$\gamma\epsilon_{x,y}$	0.6	μm
Init. slice E-spread	$\sigma_\gamma mc^2$	1	keV
BC strength	R_{56}	-135	mm
Compression factor	C	~ 13	
Final current	I_f	~ 500	A
TCAV1&2 rf frequency	$\omega/2\pi$	3.9	GHz
TCAV1 voltage	V_1	0.42	MV
TCAV2 voltage	V_2	5.22	MV
TCAV1 length	L_1	0.1	m
TCAV2 length	L_2	0.5	m

Simulations are carried out using the particle tracking code *elegant* [9]. The initial bunch is assumed to be flat-top with a peak current of 38 A and a slice energy spread of 1 keV (rms). The initial linear and quadratic chirp is set for a compression factor of about 13 across the entire bunch length. This is possible with even with compressor nonlinearity (i.e., T_{566}) by using higher harmonic rf cavities in front of the bunch compressor.

Figure 3 shows the principle of the reversible heater scheme by means of simulation of the longitudinal phase space at different locations along the beamline. The simulation includes 5×10^5 (500k) particles and the impact of coherent synchrotron radiation (CSR) is not taken into account (cf. next subsection). The initial slice energy spread is heated up in TCAV1 to 10 keV (rms), increased by the compression factor in the bunch compressor to 130 keV, and finally cooled down by TCAV2 to 13 keV. The right plot in Fig. 4 shows that the heating induced by TCAV1 is perfectly reversible and the final slice energy spread is simply the initial slice energy spread scaled with the compression factor, which is exactly like in the case without the reversible heater system. The left plot of Fig. 4 show the impact on the projected emittance of different TCAV2 voltages. The minimum of the vertical emittance is related to the cancelation of the spatial chirp and energy spread induced by TCAV1. At the minimum, the horizontal emittance is not affected at all and the small emittance growth

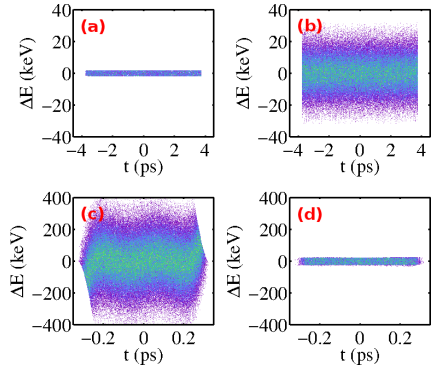

Figure 3: Simulation of the longitudinal phase space: (a) in front of TCAV1, (b) directly behind TCAV1, (c) directly behind the bunch compressor, and (d) behind TCAV2. For the sake of clarity, the axes scales change from (b) to (c).

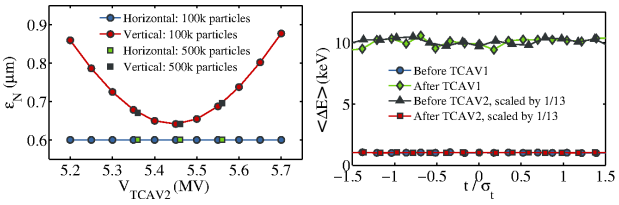

Figure 4: Simulation of the reversible-heater impact on projected emittances and slice energy spread. Top: Projected emittance (normalized). Bottom: Slice energy spread for V_{TCAV2} at minimum emittance (see above). The longitudinal coordinate is normalized to the bunch length.

in the vertical plane is due to the residual dispersion and angular dispersion generated by the system (see Eq. (7)).

Impact of coherent synchrotron radiation

The previous results undergo slight modifications when including CSR effects which is shown in Fig. 5. In comparison to the case without any CSR effects (cf. Fig. 4), the projected emittance in the vertical plane is slightly increased and the slice energy spread is not perfectly canceled in the head and tail. The slice energy spread in the core part of the bunch is also slightly increased to 18 keV (instead of 13 keV in the absence of CSR). The projected emittance in the horizontal is a factor of 2.5 larger which is independent of this heater operation. This horizontal emittance growth can be reduced by minimizing the beta function (in x) at the last dipole of the chicane where the bunch length becomes the shortest. This optimization is reserved for future studies because it does not affect the results discussed here. Nevertheless, as shown in Fig. 6, the horizontal slice emittance stays unaffected and the vertical slice emittance exhibits only deviations in the head and tail due to CSR effects. The core emittances are well preserved. The increased vertical beam size in the chicane due to TCAV1 streaking may further suppress CSR effects but require 3D CSR tracking not available in *elegant*.

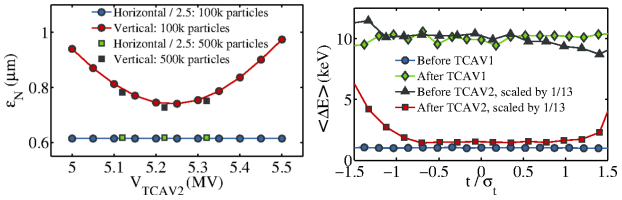

Figure 5: Simulation of the reversible-heater impact on projected emittances and slice energy spread like in Fig. 4, but including one-dimensional (projected) CSR effects.

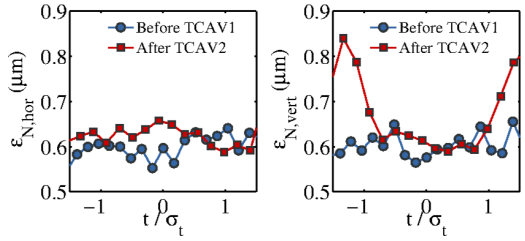

Figure 6: Simulation (500k particles) of the reversible-heater impact on the normalized slice emittance.

Microbunching studies

For practical reasons, we demonstrate the suppression of microbunching instabilities by means of a pure initial density modulation with 5% amplitude and $100\,\mu$m period ($\lambda_{\rm mod}$). This modulation is converted into energy modulations by longitudinal CSR-impedance which expresses the consistency with the analytical formalism in the previous section. Figure 7 show the longitudinal phase space behind TCAV2 for both heater switched off (top) and on (bottom). In the case without heater, strong density modulations with the compressed modulation period $\lambda_{\rm mod}/C$ appear, i.e. CSR-driven microbunching becomes visible. When switching the heater on, the microbunching instability disappears and the resulting longitudinal phase space remains smooth. We expect a similar smoothing effect if a beam with an initial energy modulation (due to LSC impedance in Linac-1) is sent to the reversible heater system.

PRACTICAL CONSIDERATIONS

A practical issue for this system is the jitter tolerance. If the electron bunch has an energy jitter on the order of 10^{-4},

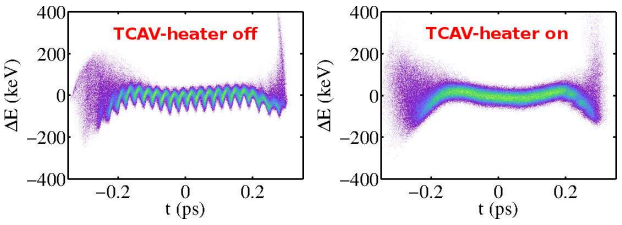

Figure 7: Simulation (1000k particles) of the reversible heater impact on CSR-driven microbunching instability.

it will experience a timing jitter of 13 μm due to R_{56} of the compressor. The bunch will arrive at TCAV2 with a phase slightly different from 90° (by 0.03°). Although TCAV2 will still be able to cancel the energy spread, it will introduce a net vertical kick to the bunch centroid that becomes a significant fraction of its angular divergence. Preliminary calculations suggest that the energy jitter should be controlled to a fraction of 10^{-4} and the TCAV2 phase jitter to 0.01° level in order to maintain good trajectory stability. This level of stability is difficult to achieve in normal-conducting linacs but may be obtained in superconducting cavities [10], especially with CW operation and active feedback systems [11].

A practical advantage with this reversible heater system is the availability of longitudinal phase space diagnostics. Time-resolved bunch properties in in the middle and after the chicane become feasible and using the incoherent synchrotron radiation, emitted in the second or third bunch compressor magnet, even a fully parasitic monitoring of the longitudinal phase space is possible.

CONCLUSIONS

Our studies show that the reversible heater system proposed here can suppress the microbunching instability and preserve the beam brightness. Due to CSR effects, some vertical emittance degradation to the head and tail parts of the bunch occurs, but the core emittance is preserved. In the numerical demonstration, the first TCAV generates about 10 keV energy spread similar to a laser heater (with a more Gaussian energy distribution than the laser heater). The bunch compression process increases the slice energy spread to 130 keV, which is then reversed to 18 keV after TCAV2 (in presence of CSR effects). Simulations also show that the initial microbunching in the beam can be smeared out during the process. Such a smooth beam can then propagate through the rest of the accelerator without generating much additional energy spread and is advantageous for any kind of laser seeding manipulations. For example, this scheme will significantly loosen the required laser power for short-wavelength HHG seeding and may strongly impact the design of future seeded FELs.

REFERENCES

[1] P. Emma *et al.*, Nature Photonics **4** 641 (2010).

[2] Z. Huang *et al.*, Phys. Rev. ST-AB **13**, 020703 (2010).

[3] C. Behrens *et al.*, THOC11, FEL2011 proceedings (2011).

[4] M. Cornacchia and P. Emma, PRST-AB **5**, 084001 (2002).

[5] D. Xiang *et al.*, WEOB4, FEL2011 proceedings (2011).

[6] M. Venturini *et al.*, PAC2011 proceedings (2011).

[7] M. Venturini and A. Zholents, NIMA **593** (2008).

[8] Z. Huang *et al.*, Phys. Rev. ST-AB **7**, 074401 (2004)

[9] M. Borland, ANL APS Report No. LS-287, 2000.

[10] C. Gerth *et al.*, THPA12, FEL2011 proceedings (2011).

[11] J. Corlett *et al.*, PAC2003 proceedings p. 2408 (2003).